ISSN 0965-545X, Polymer Science, Ser. A, 2015, Vol. 57, No. 6, pp. 889–897. © Pleiades Publishing, Ltd., 2015.

COMPOSITES

Effect of Halloysite and Maleic Anhydride Grafted Polypropylene on the Isothermal Crystallization Kinetics of Polypropylene Based Composites[1]

Zuguo Bao[a], Ellen Lee[b], Jie Tao[a], and Xianjun Sun[a]

[a] *College of Material Science and Technology, Nanjing University of Aeronautics and Astronautics, Nanjing, 210016, China*
[b] *Materials Research Department, Research and Advanced Engineering, Ford Motor Company, Dearborn, MI 48124, USA*
e-mail: taojie@nuaa.edu.cn

Received March 10, 2015;
Revised Manuscript Received May 15, 2015

Abstract—Maleic anhydride grafted polypropylene (MAPP) was incorporated into polypropylene (PP)/halloysite composites as a compatibilizer. The effect of halloysite and compatibilizer on the crystallization behavior of PP/MAPP/halloysite composites was investigated by differentical scanning calorimetry. The results indicate that Avrami crystallization theory can be used to analyze the kinetic data. As expected, the crystallinity of the composites after isothermal crystallization is higher than that after injection molding. The introduction of halloysite increases the crystallization temperature of PP by 4°C. The halloysite also promotes the nucleation and overall crystallization rate by acting as a heterogeneous nucleating agent. The incorporation of compatibilizer MAPP improves the dispersion of halloysite in the PP matrix, further facilitating the nucleation and crystallization processes. However, excess compatibilizer magnifies its negative influences on crystallization by limiting molecular mobility and diffusion and deteriorating heterogeneous nucleation. Consequently, PP/halloysite composite containing 5% compatibilizer is optimal for both the highest nucleation and overall crystallization rates.

DOI: 10.1134/S0965545X15060024

INTRODUCTION

Polymer crystallinity and crystalline morphology play important roles in physical and mechanical properties of polymers [1–3]. The analysis of crystallization kinetics can provide not only crucial information for the control of polymer based composites formulation and performance. Crystallization kinetics analysis can also provide experience for adjusting processing parameters such as cycle time in injection molding. For nanocomposites, it is necessary to understand the effect of additives on the crystallization behavior of the polymers. Generally, nanoscale fillers can boost the crystallization process owing to heterogeneous nucleation. Such promotion effect of halloysite has been confirmed by many researchers [4–7]. Nan-ying Ning investigated the crystallization behavior of PP/halloysite composites, and observed halloysite could serve as a nucleation agent, which led to an enhancement of the overall crystallization rate and the non-isothermal crystallization [8]. Baochun Guo observed the similar acceleration effect of halloysite on crystallization behavior of polyamide 6. But dissimilarly, the crystallinity of the PA6/halloysite nanocomposites increases with cooling rate. Halloysite content is found to have a significant effect upon the crystallinity of the PA6/Halloysite nanocomposites [9]. The previous research demonstrated the crystallization behavior of nanocomposite was strongly dependent on the dispersion and surface conditions.

In addition, compatibilization between the polypropylene and inorganic fillers is a common issue for nanocomposites. Maleic anhydride grafted polypropylene (MAPP) was widely used as a compatibilizer for the PP based composites to improve the inorganic filler dispersion and interfacial bonding [10, 11]. Obviously, the nucleation effect of halloysite needs to be reevaluated for the introduction of MAPP in halloysite/PP composite. On the one hand, the crystallization behavior of MAPP is different from that of PP due to the molecular structural difference, indicating heterogeneous nucleation during crystallization [12, 13]. On the other hand, the improvement of filler dispersion and interfacial bonding also influence the crystallization properties of nanocomposites [14–17]. Therefore, the crystallization behavior of the PP/MAPP/halloysite composite needs to be investigated for further understanding of the influences of halloysite.

In the present work, halloysite and MAPP are used as reinforcing filler and compatibilizer respectively in the PP based nanocomposites. The effect of halloysite and compatibilizer MAPP on the isothermal crystalli-

[1] The article is published in the original.

Table 1. Formulations of PP and its composites

	PP	MAPP	Halloysite
Neat PP	100	0	0
PP-5MAPP	95	5	0
PP-10HA	90	0	10
PP-5MAPP-10HA	85	5	10
PP-10MAPP-10HA	80	10	10
PP-15MAPP-10HA	75	15	10
PP-20MAPP-10HA	70	20	10

zation kinetics including nucleation, crystallization rate and activation energy are analyzed based on the Avrami Equation.

EXPERIMENTAL

Materials

Isotactic PP (Pro-Fax 6523, Lyondell Basell) with a density of 0.90 g/cm^3 and a melt flow index 4.0 g/10 min (ASTM D 1238) was used for the polymer matrix. Halloysite (Dragonite-HP: KF) was provided by Applied Minerals Inc., and used without further treatment. Maleic anhydride grafted polypropylene (Polybond 3200, Chemtura) with a maleic anhydride level of 1.0 wt% was utilized as a compatibilizer in the composite. The formulations of the composites are listed in Table 1.

Extrusion and Injection Molding

PP, MAPP and halloysite were blended by twin-screw extrusion (Thermo Scientific, Haake Polylab System). Halloysite was pre-dried at 110°C for 1 h to remove the surface moisture before extrusion. The temperature profile for the eight heating zones from the hopper to the die was 180/180/185/190/195/200/205/210°C. The composite strands were cooled through a water bath and pelletized. The pellets were dried for 24 hours at 70°C and then injection molded in an 80-ton injection press (BOY Machines, 80 M). The injection molding barrel temperature profile from feed zone to nozzle was 200/200/200/205/205°C.

Microstructure Characterizations

Fracture morphology and clay dispersion were observed by JEOL 6610 Scanning Electron Microscope with an accelerating voltage of 10 kV. The specimen was coated with a carbon film to improve its conductivity.

Crystallization Measurements

The isothermal crystallization of PP/halloysite composites was measured by differential scanning calorimetry (DSC) on a DSC/STARe system from Mettler Toledo, Switzerland. All DSC measurements were performed under nitrogen purging. The specimens were first heated from room temperature to 210°C at a heating rate of 10°C/min and held at this temperature for 5 minutes to erase the heat history from previous processes. The specimens were then cooled to the desired isothermal crystallization temperature (ranging from 126 to 138°C) at a rate of 20°C/min and held for 30–90 minutes. Heat flows of the specimens after isothermal crystallization were also recorded.

Crystalline content of the injection molded specimens were measured by DSC to assess the content expected from a real-life non-isothermal crystallization process. Heat flows and crystalline content were also compared to those from isothermal crystallization.

RESULTS AND DISCUSSION

Crystallinity

Figure 1 exhibits DSC thermograms of the neat PP sample during isothermal crystallization. The polymer crystallinity of specimens with a heat history of injection molding and after isothermal crystallization, $X_{c(inj)}$ and $X_{c(iso)}$, respectively, are calculated from corresponding melting curves based on the expression below:

$$X_c = \Delta H_m / \Delta H_m^\theta, \quad (1)$$

where ΔH_m stands for the melting enthalpy of the given specimen, while ΔH_m^θ corresponds to the melting enthalpy for 100% crystallized polymer. For PP, $\Delta H_m^\theta = 209$ J/g.

The calculated results are summarized in Table 2. The crystallinity of PP after isothermal crystallization ($X_{c(iso)}$) is obviously higher than that of the non-isothermally crystallized injection molded sample ($X_{c(inj)}$). The typical difference is approximately 6–10%, which is almost one fifth of the total crystallinity. This is caused by the complexity of polymer crystallization. The nucleation and growth rates are very sensitive to molecule mobility determined by temperature and time. The higher supercooling degree and shorter crystallization time provided by the injection molding process limit the mobility and diffusion of polymer molecules, causing some crystallizable material to solidify before crystal formation and ultimately a lower crystalline content. Isothermal crystallization offers better molecular mobility and diffusion for the polymer, resulting in a higher crystallinity. The crystallinity after isothermal crystallization increases with the raising crystallization temperature, T_c. The change of peak temperature, T_p, and crystallization enthalpy, H_{total}, with T_c also

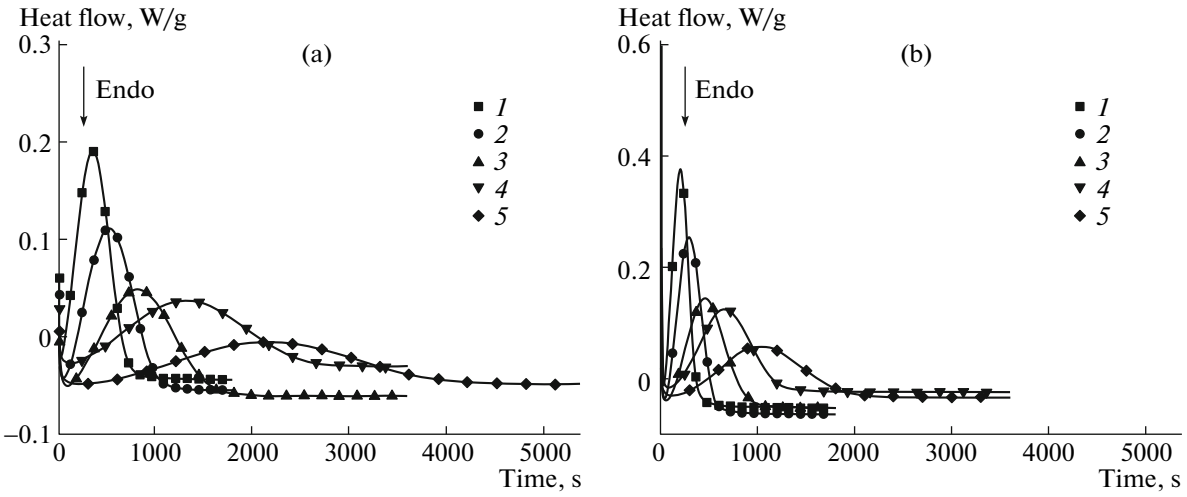

Fig. 1. DSC thermograms of isothermal crystallization for (a) neat PP at (*1*) 126, (*2*) 128, (*3*) 130, (*4*) 132 and (*5*) 134°C and (b) PP-5MAPP-10HA at (*1*) 130, (*2*) 132, (*3*) 134, (*4*) 136 and (*5*) 138°C.

confirm this conclusion. For the samples containing halloysite, their crystallinity levels are higher than that of pure PP, suggesting a promotion effect of halloysite on polymer crystallization. Such promotion plays an important role in the reinforcing effect of halloysite for PP since crystallinity is a key factor that determines the mechanical properties of polymers.

Relative Crystallinity

From the relationship between heat-flow and crystallization time, the relative crystalline fraction by weight, X_w, at moment t can be calculated by

$$X_w = \frac{\Delta H(t)}{\Delta H_{\text{total}}} = \frac{\int_{t_i}^{t}(dH/dt)dt}{\int_{t_i}^{t_e}(dH/dt)dt}, \quad (2)$$

where t_i and t_e denote the moments when the measurable crystallization initiates and ends, respectively. They are determined by curves in Fig. 1. Thus, the relative crystalline fraction by volume, X_v, can be calculated by

$$X_v = \frac{X_w}{X_w + (1 - X_w)\rho_c/\rho_a}, \quad (3)$$

where ρ_c and ρ_a are the densities of crystalline and amorphous polymer, respectively. Considering the influence of temperature, the ratio of ρ_c/ρ_a can be modified by the following empirical equation [18]:

$$\frac{\rho_c}{\rho_a} = \left(\frac{\rho_{co}}{\rho_{ao}}\right)\exp\left[(T - 298)\left(\frac{0.16}{T_g} - \frac{0.11}{T_m}\right)\right], \quad (4)$$

where ρ_{co} and ρ_{ao} are the densities of crystalline and amorphous polymer at a reference temperature of 298 K, respectively. T_m and T_g refer to the equilibrium melting point and glass transition temperature, respectively. For PP [19], $\rho_{co} = 0.936$ g/cm^3, $\rho_{ao} = 0.85$ g/cm^3, $T_m = 444.2$ K, and $T_g = 256.2$ K.

Based on these manipulations, the crystalline volume fraction can be calculated as a function of time, see Fig. 2. To control the crystallization at a measurable window (in the range of 10 minutes to 2 hours), nanocomposite samples isothermally crystallize at higher (by 4°C) temperatures than those for the neat PP. The general shapes of isotherms are qualitatively in accord with Avrami model at the starting and developing periods [18]. The decreased crystallization rate in the "tail region" mainly results from the impingement of spherulites when crystallized polymer grows to a considerable fraction, showing that crystallization temperature plays an extremely important role in the crystallization. The complete crystallization time is almost doubled with every 2°C increment.

Overall Crystallization Kinetics

The overall crystallization kinetics of polymer can be analyzed by Avrami equation [20]:

$$X_v(t - t_i) = 1 - \exp[-K^*(t - t_i)^n], \quad (5)$$

where $X_v(t - t_i)$ is the volume fraction crystallinity in the crystallizable material at time t. Here induction time, t_i, is introduced to exclude the time period before the crystallization starts. $X_v(t - t_i)$ could be calculated by Eq. (3). K is crystallization rate constant and is a function of temperature. The Avrami exponent n, contains information about nucleation and growth geometry.

Table 2. Isothermal crystallization kinetics of PP/halloysite composite

Crystallization properties	T_c, °C	$X_{c(inj)}$, %	$X_{c(iso)}$, %	T_p, °C	ΔH_{total}, J/g	t_i, s	K, $10^3 \times min^{-n}$	n	$t_{1/2}$, min	ΔE, kJ/mol
Neat PP	126	35.90	46.30	164.54	81.56	46	0.009	2.45	5.82	−300.59
	128	36.75	47.16	164.79	82.82	74	0.0032	2.54	8.27	
	130	35.46	48.32	164.32	83.57	112	0.0012	2.50	12.97	
	132	37.15	47.92	165.34	84.66	138	2.8×10^{-4}	2.56	21.15	
	134	37.00	48.16	166.17	88.72	229	4.1×10^{-5}	2.75	34.30	
PP-5MAPP	126	38.21	47.10	163.04	88.11	31	0.011	2.91	4.13	−341.93
	128	37.15	48.47	163.59	88.96	59	0.0035	2.85	6.39	
	130	38.78	47.61	164.51	90.56	88	7.4×10^{-4}	2.87	10.83	
	132	38.18	49.29	165.06	92.20	125	1.0×10^{-4}	3.01	18.52	
	134	38.62	48.84	166.18	92.83	221	2.7×10^{-5}	2.97	30.68	
PP-10HA	130	38.21	48.62	164.51	84.47	36	0.038	3.29	2.42	−401.40
	132	39.50	47.54	165.07	87.63	56	0.0046	3.36	4.46	
	134	38.92	48.31	165.95	87.08	102	0.00069	3.28	8.23	
	136	39.46	49.30	167.09	87.99	155	0.00010	3.27	14.84	
	138	39.32	49.36	168.03	90.33	323	0.00005	3.02	24.13	
PP-5MAPP-10HA	130	40.65	49.00	164.66	80.78	31	0.038	2.60	3.06	−284.69
	132	40.50	49.38	165.03	83.09	39	0.0136	2.59	4.55	
	134	39.27	51.50	165.77	83.88	58	0.0036	2.65	7.25	
	136	39.74	49.76	167.08	85.12	88	1.1×10^{-3}	2.76	10.24	
	138	40.27	50.63	166.69	85.38	123	2.9×10^{-4}	2.79	16.31	
PP-10MAPP-10HA	130	40.26	48.91	164.09	84.35	30	0.030	2.76	3.13	−342.20
	132	40.57	47.22	164.65	83.58	37	0.0083	2.74	5.01	
	134	41.41	46.52	166.01	86.97	70	1.6×10^{-3}	2.88	8.13	
	136	40.48	47.65	166.61	86.70	103	4.4×10^{-4}	2.84	13.35	
	138	39.39	49.36	167.75	88.47	124	9.2×10^{-5}	2.84	23.11	
PP-15MAPP-10HA	130	42.31	48.20	163.85	84.59	30	0.011	2.89	4.20	−341.55
	132	42.60	47.40	164.61	85.60	64	0.0026	2.87	7.01	
	134	40.90	49.31	165.44	86.70	93	7.7×10^{-4}	2.82	11.19	
	136	40.89	48.56	166.33	90.13	100	8.2×10^{-5}	3.03	19.68	
	138	40.90	51.18	167.49	89.77	180	4.3×10^{-5}	2.85	29.95	
PP-20MAPP-10HA	130	38.40	47.23	164.53	73.86	79	0.011	2.80	4.37	−359.19
	132	39.23	47.86	164.48	88.03	77	0.0017	2.85	8.24	
	134	39.00	49.33	165.56	88.39	139	0.0004	2.91	13.44	
	136	41.73	50.55	166.45	91.10	163	6.5×10^{-5}	2.96	22.94	
	138	41.62	49.52	167.33	92.45	312	3.3×10^{-5}	2.79	35.55	

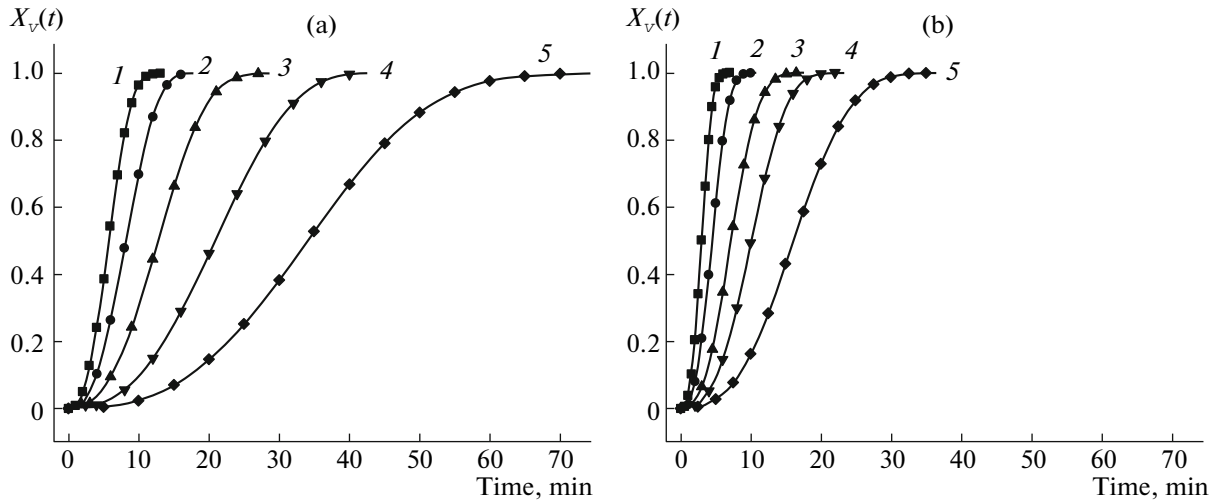

Fig. 2. Relative crystallization fraction by volume vs. time for (a) neat PP at (*1*) 126, (*2*) 128, (*3*) 130, (*4*) 132, and (*5*) 134°C and (b) PP-5MAPP-10HA at (*1*) 130, (*2*) 132, (*3*) 134, (*4*) 136, and (*5*) 138°C.

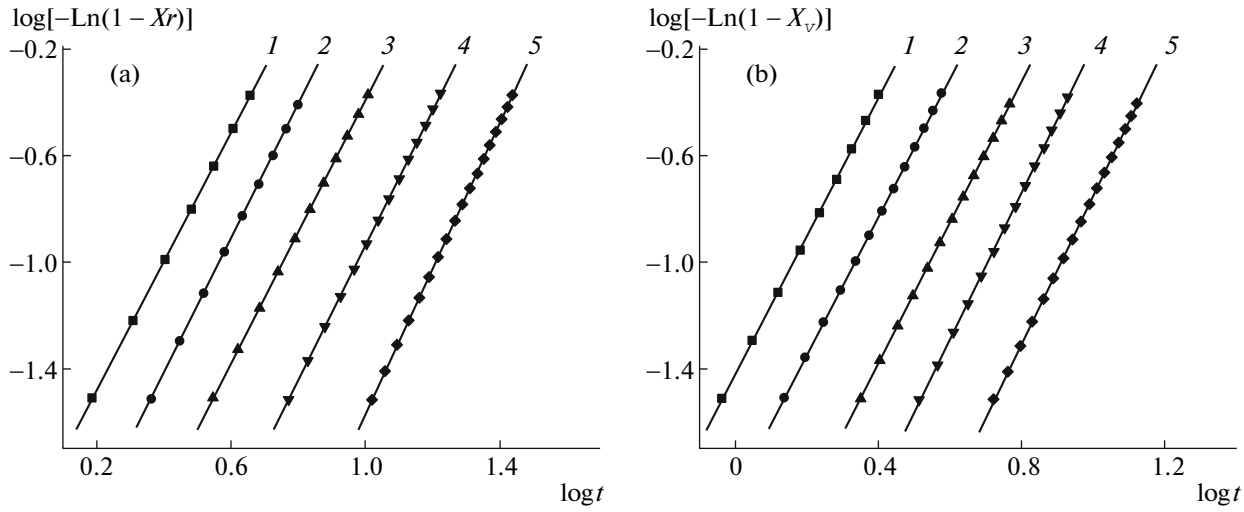

Fig. 3. Plots of log[−ln[1 − $X_v(t - t_i)$]] as a function of log*t* for (a) neat PP at (*1*) 126, (*2*) 128, (*3*) 130, (*4*) 132, and (*5*) 134°C, and (b) PP-5MAPP-10HA at (*1*) 130, (*2*) 132, (*3*) 134, (*4*) 136, and (*5*) 138°C.

Applying logarithmic calculation to Eq. (5), one can obtain the following equation:

$$\log[-\ln[1 - X_v(t - t_i)]] = \log K + n\log(t - t_i). \quad (6)$$

From a graphic representation of log[−ln[1−$X_v(t - t_i)$]] versus log*t* in Fig. 3, the Avrami exponent, *n*, (slope of the straight line) and isothermal crystallization kinetic constant *K* (intersection with the *y*-axis) can be calculated. Here, only the linear portion at low relative crystallinity region (3–35%) is applied for linear fitting. The good linear relationship shown in Fig. 3 also reveals the applicability of Avrami theory on the crystallization of PP/halloysite composites.

In addition, crystallization half-time, $t_{1/2}$, is commonly defined to evaluate the overall crystallization rate. Substituting $X_v(t - t_i) = 0.5$ in Eq. (5), one can obtain:

$$t_{1/2} = (\ln 2/K)^{1/n}. \quad (7)$$

The overall crystallization properties are summarized in Table 2. The crystallization process consists of two steps: nucleation and crystal growth. The overall crystallization rate is determined by the nucleation rate and spherulitic growth rate. Induction time, t_i, crystallization rate constant, *K*, and crystallization half-time, $t_{1/2}$, are plotted in Fig. 4. Induction time reflects the nucleation capability of the supercooled polymer. Small induction time at higher crystalliza-

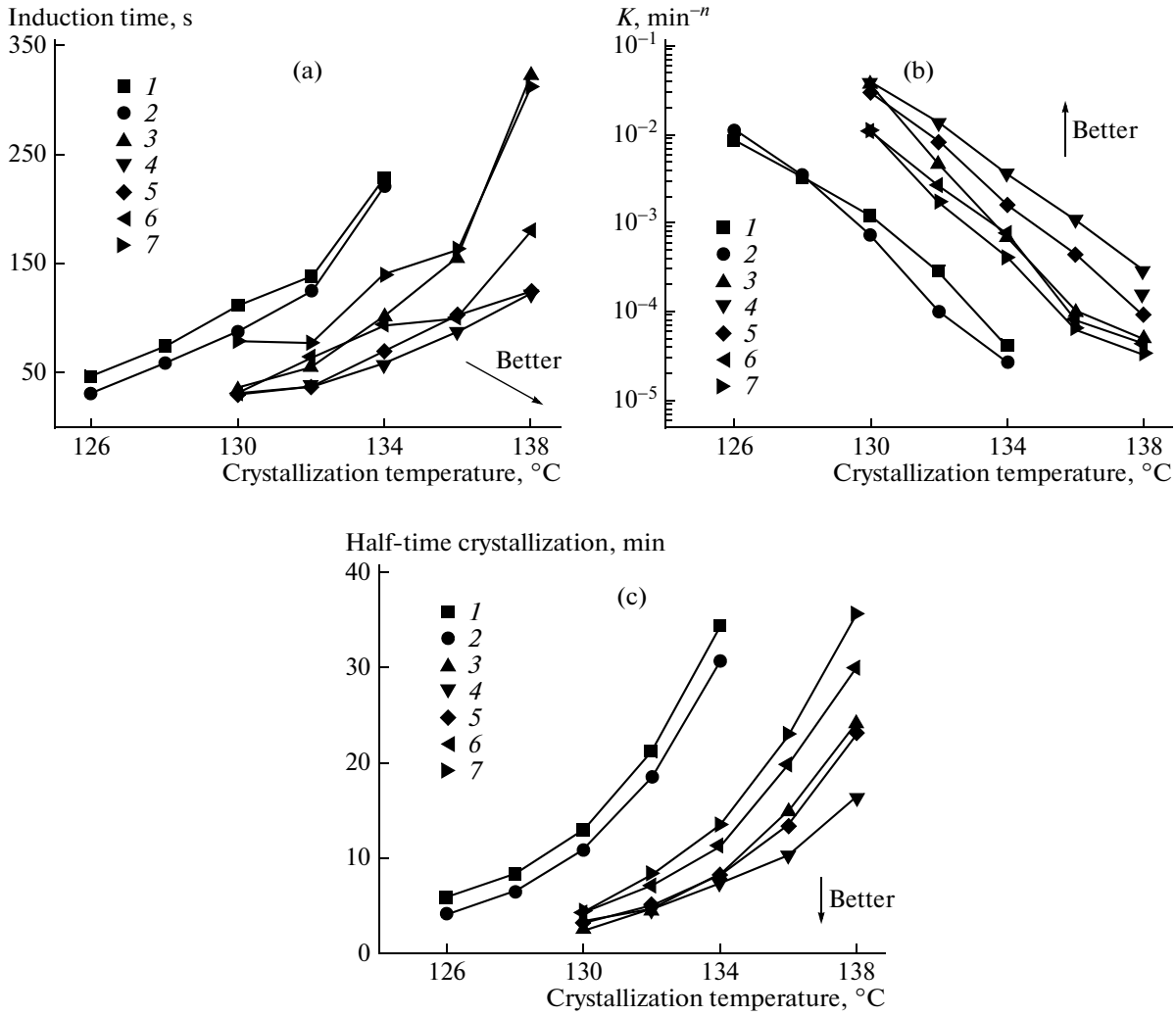

Fig. 4. (a) Induction time, (b) crystallization rate constant, and (c) crystallization half-time vs. crystallization temperature for PP and its composites: (*1*) neat PP, (*2*) PP-5MAPP, (*3*) PP-10HA, (*4*) PP-5MAPP-10HA, (*5*) PP-10MAPP-10HA, (*6*) PP-15MAPP-10HA, and (*7*) PP-20MAPP-10HA.

tion temperature is preferred for strong nucleation ability by creating more nucleation centers, possibly forming a fine-crystal structure. Another advantage of a small induction time lies in shortening the cycle time for polymer processing (e.g. injection molding). The induction time of PP/halloysite composites is summarized in Fig. 4a. Apparently, when the polymer crystallizes at higher temperatures, nucleation rate is depressed as the initiation time, t_i, is fairly prolonged. It is reasonable since the critical size of nucleus increases when the supercooling degree gets smaller (higher crystallization temperature) [21]. In addition, the spherulitic growth of PP is also negatively dependent on the temperature, based on the theoretical research [22]. Therefore, the overall crystallization rate, observed from crystallization rate constant K, and crystallization half-time $t_{1/2}$, is negatively dependent on the temperature for the same material.

At the same temperature, PP-5MAPP displays shorter induction time and smaller rate constant, which indicates it possesses a higher nucleation rate but lower overall crystallization rate. Therefore, the spherulitic growth rate in PP-5MAPP is lower than that of neat PP. The possible reason is that steric hindrance and hydrogen bond introduced by maleic anhydride impedes the mobility and diffusion of polymer molecules during crystallization.

Compared with MAPP, the halloysite shows a much stronger influence on the PP crystallization. As mentioned before, the introduction of halloysite in the composite elevates the crystallization temperature by approximately 4°C. Furthermore, the crystallization rate of halloysite filled composite is also much higher than that of PP at the same temperatures. Halloysite acts as a heterogeneous nucleating agent in the molten polymer, promoting the nucleation rate significantly. This promotion effect is enhanced by the incorpora-

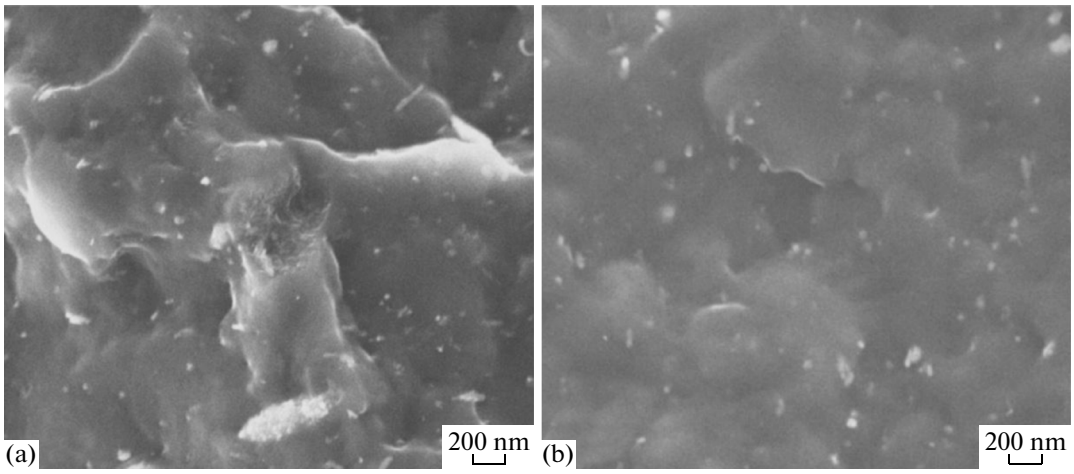

Fig. 5. SEM images of PP/halloysite composite: (a) without MAPP; (b) with 5% MAPP.

tion of compatibilizer MAPP in halloysite filled PP. As shown in Fig. 5, the compatibilizer can improve clay dispersion in the polymer matrix, providing more nucleation centers from the smaller, dispersed halloysite particles. More importantly, such improvement in nucleation can be well maintained at higher crystallization temperatures, which is confirmed by the shorter induction time t_i, of PP/MAPP/halloysite composite in Table 2 and Fig. 4a.

It is worth noting, however, that too much MAPP is ineffective in further promoting crystallization. On the one hand, MAPP contains polar functional groups (C=O) that could interact with the halloysite surface. The crater in the center of Fig. 5a, which displays an apparent rough surface, is tearing interface between halloysite aggregate and PP matrix. This damage pattern and clay aggregates are largely alleviated with the introduction of MAPP (Fig. 5b). However, excess compatibilizer offers negligible improvement in clay dispersion, but may in fact hinder the heterogeneous nucleation by forming coated shells on the clay particles. This core-shell structure was observed in PP/halloysite composite with high compatibilizer content, as displayed in Fig. 6. Furthermore, the introduced MAPP will impede the movement of PP molecules. The more the MAPP is introduced in polymer, the poorer the molecular mobility becomes. Therefore, the content of MAPP has an optimal value for maximizing the heterogeneous nucleation of halloysite in the composites. Based on the experimental results, PP-5MAPP-10HA displays the smallest induction time and crystallization half-time as well as the largest crystallization rate constant, exhibiting both the highest nucleation rate and overall crystallization rate. In other words, PP-5MAPP-10HA reaches the optimal balance between improving clay dispersion and nucleation and limiting the negative effects of impeding PP molecular diffusion.

Activation Energy

Kinetic parameters are determined by the Arrhenius equation [23]:

$$K^{1/n} = k_0 \exp[-\Delta E/(RT_c)], \quad (8)$$

where k_0 is the pre-exponential factor, ΔE is the activation energy of crystallization, and R is the gas constant. Eq. (8) can be changed to

$$(1/n)\ln K = \ln k_0 - \Delta E/(RT_c). \quad (9)$$

From a plot of $(1/n)\ln K$ versus $1/(RT_c)$, the activation energy ΔE, and the coefficient, $\ln k_0$, can be determined from the slope and y-intercept of the linear fitted line, respectively (see Fig. 7).

The activation energy is summarized in Table 2. It should be pointed out that the calculated activation energy is a negative value since the crystallization rate possesses a negative temperature-dependent feature. (Strictly speaking, positive temperature dependence of crystallization rate does exist for most

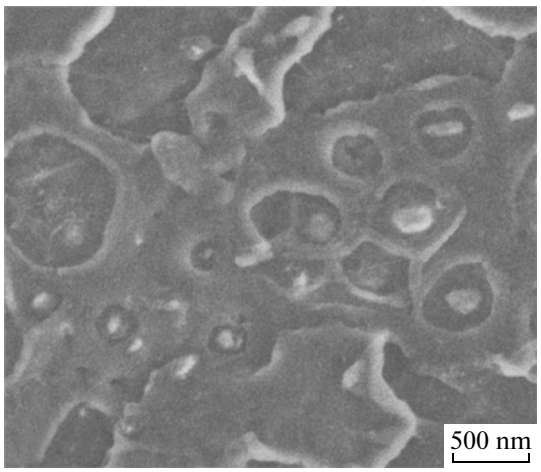

Fig. 6. Halloysite particles in PP-20MAPP-10HA.

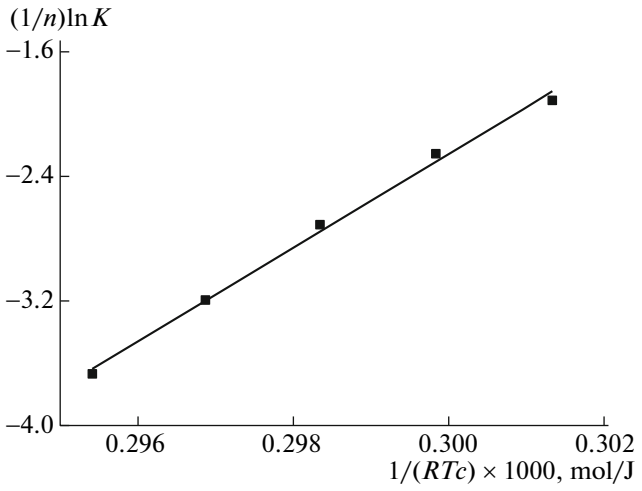

Fig. 7. Plot of $(1/n)\ln K$ as a function of $1/(RT_c)$ for neat PP.

of polymers theoretically. They could be obtained if the polymer crystallizes at a very slow rate by a large supercooling. For PP in our experimental temperature window, crystallization rate is negatively dependent on temperature [24]). For comparison of different materials, activation energy can only reflect the temperature effect on crystallization rate on account of different pre-exponential factors. For comparison of the same material, activation energy can additionally be used for comparing crystallization rate. As shown in Table 2, the introduction of compatibilizer can reduce the activation energy of PP-halloysite. Therefore, its introduction simultaneously increases the crystallization rate and depresses its negative temperature dependence. The activation energy increases as the loading level of MAPP increases, indicating that excess compatibilizer can deteriorate the improvement of PP crystallization brought by the addition of halloysite. This analysis is also consistent with the above results.

CONCLUSIONS

The isothermal crystallization kinetics of PP and PP/halloysite composites was investigated by DSC. The crystallinity of PP after isothermal crystallization was significantly higher than that after injection molding. The kinetic data were calculated and analyzed by Avrami crystallization theory. The crystallization temperature of PP was elevated by 4°C with the introduction of halloysite. The halloysite promoted the nucleation and overall crystallization rates, by acting as a heterogeneous nucleating agent. The incorporation of compatibilizer MAPP improved the dispersion of halloysite, further facilitating the nucleation. An optimized content of compatibilizer shortened the induction time for crystallization and boosted the crystallization rate. However, the negative influences of MAPP dominated if redundant content was added into the formulation. Such influences brought by MAPP included the limitation of molecular mobility and diffusion in PP melt, and deterioration of heterogeneous nucleation by forming coated shells on halloysite particles. As a result, PP/halloysite composite with 5% of MAPP displayed both the highest nucleation and overall crystallization rates. The calculated activation energy was also consistent with the results of kinetics analyses.

ACKNOWLEDGMENTS

This work was supported by Ford China University Research Program (no. 2009-5041R), Funding of Jiangsu Innovation Program for Graduate Education (no. CXLX11_0189), Nanjing University of Aeronautics and Astronautics Research Funding (no. 1006-KFA13731) and A Project Funded by the Priority Academic Program Development of Jiangsu Higher Education Institutions (PAPD). The authors appreciate Applied Minerals for the supply of halloysite clay used in this study.

REFERENCES

1. T. Parenteau, G. Ausias, Y. Grohens, and P. Pilvin, Polymer **53**, 5873 (2012).
2. A. Galeski, Prog. Polym. Sci. **28**, 1643 (2003).
3. J. Varga, J. Macromol. Sci. Part B: Phys. **41**, 1121 (2002).
4. M. Du, B. Guo, J. Wan, Q. Zou, D. Jia, J. Polym. Res. **17**, 109 (2010).
5. M. Liu, Y. Zhang, and C. Zhou, Appl. Clay Sci. **75**, 52 (2013).
6. B. Wang and H. Huang, Polym. Degrad. Stab. **98**, 1601 (2013).
7. M. Liu, B. Guo, M. Du, F. Chen, D. Jia, Polymer **50**, 3022 (2009).
8. N. Ning, Q. Yin, F. Luo, Q. Zhang, R. Du, Q. Fu, Polymer **48**, 7374 (2007).
9. B. Guo, Q. Zou, and Y. Lei, Thermochim. Acta **484**, 48 (2008).
10. G. Gong, B. Xie, and W. Yang, Polym. Test. **25**, 98 (2006).
11. S. Zhu, J. Chen, Y. Zuo, H. Li, Y. Cao, Appl. Clay Sci. **52**, 171 (2011).
12. Y. Seo, J. Kim, and K. Kim, Polymer **41**, 2639 (2000).
13. K. Cho, F. Li, and J. Choi, Polymer **40**, 1719 (1999).
14. R. Nowacki, B. Monasse, E. Piorkowska, A. Galeski, J. M. Haudin, Polymer **45**, 4877 (2004).
15. W. Xu, G. Liang, H. Zhai, S. Tang, G. Hang, W. Pan, Eur. Polym. J. **39**, 1467 (2003).

16. J. Li, C. Zhou, and W. Gang, Polym. Test. **22**, 217 (2003).

17. M. Du, B. Guo, M. Liu, and D. Jia, Polym. J. **38**, 1198 (2006).

18. K. Chuah, S. Gan, and K. Chee, Poymer **40**, 253 (1998).

19. *Polymer Handbook, Fourth ed.*, Ed. by J. Brandrup, E. Immergut, and E. Grulke, (Wiley-interscience, New York, 1999).

20. L. Mandelkern, *Crystallization of Polymers: Volume 2, Kinetics and Mechanisms, Second ed.* (Cambridge University Press, Cambridge, 2004).

21. B. Wunderlich, *Macromolecular Physics, Volume 2: Crystal Nucleation, Growth, Annealing* (Acad. Press, New York, 2005).

22. L. Mandelkern, N. Jain, and H. Kim, J. Polym. Sci., Part A-2 **6**, 165 (1968).

23. P. Cebe and S. Hong, Polymer **27**, 1183 (1986).

24. A. Gandica and J. Magill, Polymer **13**, 595 (1972).